Royal Norwegian Council
for Scientific and Industrial Research
(NTNF)

NORSAR

NORSAR Scientific Report No. 2-90/91

Semiannual Technical Summary

1 October 1990 — 31 March 1991

Kjeller, May 1991

7.7 Initial development of generic relations for regional threshold monitoring

Introduction

In earlier reports (Kværna and Ringdal, 1990a, Kværna and Ringdal, 1990b) we have demonstrated applications of the threshold monitoring (TM) technique to regions of limited areal extent like mines and nuclear test sites. This method has proven to provide a simple and very effective tool in day-to-day monitoring of areas of particular interest. One of the basic underlying assumptions has been that each target region should be defined such that all events within the region show similar propagation characteristics. This has enabled us to get the necessary magnitude calibration factors from processing previous events with "known" magnitude, using the relation

$$\hat{b}_{i,j} = \hat{m}_j - \log(\hat{S}_{i,j}) \qquad (i = 1, \cdots, K;\ j = 1, \cdots, L) \tag{1}$$

where $\hat{b}_{i,j}$ is our estimate of the magnitude correction factor for phase i and event j, $\hat{m}_j$ is the estimate of the magnitude for event j (based on independent networks or knowledge about the explosive charge) and $\hat{S}_{i,j}$ is our estimate of the signal level at the predicted arrival time of phase i for event j. K is the number of phases considered (there might be several stations and several phases per station), and L is the number of events.

The magnitude correction factor to be used for phase i is then given by

$$b_i = E < \hat{b}_{i,j} > \tag{2}$$

where E denotes statistical expectation. Parameters like window lengths for signal level estimation, travel-times of the different phases, frequency filters and steering delays for array beamforming are taken from processing of the calibration events.

Extension of the TM method to regions where no calibration events are available, requires that we have generic formulas for all variables describing the processing. Such relations will make it possible to monitor new and larger geographical regions, and will in addition enable us to get a more thorough understanding on how events originating in one region influence the threshold in other regions. Applying such generic relations will of course involve a tradeoff where a wider geographical coverage is achieved at some expense with regard to optimized monitoring of limited target area. Thus it should be seen as a supplement, and not a replacement of, the target-specific threshold monitoring.

In the following we present results from a preliminary study on methods for obtaining such generic relations, with special application to the regional Fennoscandian array network.

Phases to consider and their travel-times

A standard method of estimating the magnitude of local and regional events is based on a measurement of the amplitude of the maximum peak in the S-wavetrain (Richter, 1935; Båth, 1981; Alsaker *et al*, 1990). The NORSAR recordings of Fig. 7.6.1 show that the position of the maximum peak vary strongly from one region to another. Events originating within the Fennoscandian Shield (event 1 and event 5) will usually have the maximum energy associated with the L_g phase (group velocity 3.5 km/s). On the other hand, events with propagation paths crossing the North Sea graben structures (event 4) or events originating in oceanic regions (event 6) will have the their maximum energy associated with the S_n arrival (group velocity about 4.5 km/s). In addition, Kværna and Mykkeltveit (1985) have shown that the regions in which the L_g arrival is the dominant phase are dependent on the frequencies considered. I.e., the S_n phase becomes more dominant as the frequencies increase.

The TM method require that the travel-times of the considered phases are given á priori for all target areas. For optimum performance, one phase should be associated with the energy maximum of the wavetrain. From the complexities described above, it is obvious that we cannot obtain generic formulas for the travel-time of this amplitude peak without extensive data analysis and regional mapping. For NORESS recordings, we have from the study of Kværna and Mykkeltveit (1985) an idea of the geographical regions for which S_n or L_g is the dominant phase, but similar information is currently not available for other seismic arrays and single stations.

From several years of experience with seismic data from local and regional events, we know that the energy associated with the P-phase often exhibits its amplitude maximum several seconds after the initial P onset. This feature is partly illustrated in Fig. 7.6.1. For optimum TM computations, it is also beneficial to make use of the phases for which the travel-time difference is as large as possible. We will therefore in the following proceed with the first arriving P-phase (P_n or P_g) and the L_g phase in the TM analysis, using the standard Fennoscandian travel-time tables as the generic formulas. To compensate for the uncertainties in the positioning of the maximum amplitudes of the wavetrain, we will introduce so-called time tolerances. This concept will be outlined in one of the following sections.

Frequency bands

To ensure optimum performance of the TM method, we introduce bandpass filtering of the data in the band where the considered phase is expected to have the largest SNR. These bands are however difficult to predict as large variations occur regarding attenuation properties of the different propagation paths, source

spectra and noise conditions.

In the context of monitoring regions within local and regional distances, the work of Sereno (1991) gives an excellent picture of the average properties of regional phase attenuation, source spectral scaling and backgound noise conditions. From an assumption on the event magnitude M_L and the epicentral distance, we could use his results to predict the best SNR frequency band of a phase.

We will, however, in this preliminary study base our selection of filter bands on statistics from the detection processing of the regional arrays NORESS and ARCESS. The IAS/IMS system (Bache *et al*, 1990) is used for routine analysis of data from these arrays, and all information concerning the detected seismic phases are stored in a large data base. The statistics on the dominant frequency, i.e., the frequency with the largest SNR, give us an idea on how the optimum frequency band varies as a function of epicentral distance. The statistics cover both NORESS and ARCESS data from the time interval 1990/01/23 to 1991/04/29.

The P_n (P_g) results are given in Table 7.6.1, and show large variability, especially at distances below 500 km. At larger distances the frequency band 3 to 5 Hz cover the vast majority of the occurrences. To retain simplicity in this preliminary study, we have chosen to use the 3 to 5 Hz frequency band for the first arriving P-phase at all distances. For larger distances this is also in general agreement with predictions based on the results of Sereno (1991).

The L_g results given in Table 7.6.2 also show large variability at distances below 500 km. It should be noted that the dominant frequencies for L_g are relative to the preceding S_n coda, and not relative to backgound noise conditions, as was the situation for P_n. We want optimum performance relative to backgound noise conditions, so the L_g statistics should be interpreted with some caution. On the other hand, numerous studies of L_g propagation characteristics (a.o., Baumgardt, 1990; Sereno, 1991; Kværna and Mykkeltveit, 1986) confirm the "low-frequency" nature of L_g at distances above 500 km. Also in this case we will make a compromise and use the 1.5 to 3.5 Hz frequency band for L_g at all distances. This will give close to optimum performance for L_g at longer distances, which is considered the most important for the overall threshold monitoring capability.

Grid definitions and time tolerances

Threshold monitoring of a larger geographical region implies that each target point have to represent a finite surrounding area. If we divide the region to be monitored into a grid, as shown in Fig. 7.6.2, the area surrounding the target point is given by a rectangle as indicated on the same figure.

The travel-time of the considered phase is given by T_Δ, where Δ denote the distance from the station A to the target point M. Let T_{Δ_1} be the minimum

travel-time from any point within the rectangle, e.g., $M1$, and let T_{Δ_2} be the maximum travel-time from any point within the rectangle, e.g., $M2$.

If the density of the grid is such that the magnitude calibration factors do not vary significantly within the rectangle surrounding each grid point (see Fig. 7.6.2), we use the following procedure for monitoring:

Let $S(t)$ denote the signal level observed at time t. Instead of measuring the signal level at time T_Δ as predicted from the position of the target point, we introduce time tolerances such that

$$S(T_\Delta) = \max(S(t)) \tag{3}$$

where $t \in [T_{\Delta_1}, T_{\Delta_2}]$. Thereby the estimated signal level can be said to represent an upper limit for any sources within the rectangle. The time tolerances can also be used to compensate for uncertainties in the position of the maximum amplitude of the wavetrain, but we note that the resolution of the TM method will be deteriorated if the time tolerances becomes too large.

STA lengths

In determining the optimum STA window length, we need to take three factors into account:

- Average STA during noise conditions.
- Variability of STA during noise conditions.
- Maximum STA value when the signal occurs.

In practice, it is desirable to have a signal-to-noise ratio as large as possible, measured relative to multiples of the noise standard deviation. Our approach toward solving this problem is outlined in the following.

In this initial study, we have chosen to sample the data by 1 second short-term-averages (STA) sampled at 1 second intervals. This decision is based on a compromise between data resolution and managable data volumes.

Intuitively, an instantaneous phase with short duration (e.g., P_n) should be represented by an STA averaged of a short time window, whereas the amplitude level of an emergent phase with long duration (e.g., L_g) should be represented by a longer time window. The initial data sampling (1 sec. STA values), allows us to use any integer multiple of 1 second as window lengths for the considered phases.

Let $\overline{A}(\Delta t)$ denote the average of the $\log(STA)$ under noise conditions, and let $\sigma(\Delta t)$ be the associated standard deviation. Δt refers to a particular STA

window length. Let $y(\Delta t)$ be what we consider the "worst case" noise situation given by

$$y(\Delta t) = \overline{A}(\Delta t) + x \cdot \sigma(\Delta t) \tag{4}$$

Let $S(\Delta t)$ be the maximum of $\log(STA)$ for the signal. We introduce the term "noise damping", $z(\Delta t)$ by the formula:

$$z(\Delta t) = S(\Delta t) - y(\Delta t) \tag{5}$$

The "noise damping" is then a measure of the "effective" signal-to-noise ratio, i.e., how much the signal exceeds the "worst case" noise situation. The optimum STA window length, Δt, is the argument for which the noise damping $z(\Delta t)$ attains its maximum.

To assess the optimum STA window lengths for P_n and L_g and to reveal any distance dependency, we computed maximum signal STA values with different window lengths for events at various epicentral distances.

Using the z-component of the center instrument of NORESS, ARCESS or FINESA, the P_n data were filtered in the 3-5 Hz passband. The starting point of the STA windows were at the predicted arrival time of the P-phase, and to accomodate for uncertainties in the positioning of the amplitude maximum of the P-wavetrain, we introduced a time tolerance of $\pm$ 5 seconds. Information on the P_n data are given in Table 3. The interpolated curves of Fig. 7.6.3 give $S(\Delta t)$ for several events for a set of different window lenghts. For this study, the absolute scale of $S(\Delta t)$ is without any significance, so for display purposes, an offset was added to each of the curves. As expected, the shortest window length (1 second) gave the largest $S(\Delta t)$, but there is a distinct difference in the slopes for events above and below 300 km epicentral distance. We will therefore in the following proceed with two average signal curves, one for all events within 300 km of the stations, and another for for the rest.

The noise characteristics for the 3-5 Hz frequency band was obtained from analysis of six 30 minute noise intervals. Information on the noise intervals are given in Table 7.6.4. For consistency with the P_n analysis, a time tolerance of 5 seconds was used. Values of $\overline{A}(\Delta t)$ for all noise samples are given in Fig. 7.6.4, together with the average over all six samples. Similar curves for $\sigma(\Delta t)$ are given in Fig. 7.6.5.

Now turning to the noise damping of the P_n phase for events within 300 km of the station. Fig. 7.6.6 give the noise damping $z(\Delta t)$ for a set of confidence levels $x \cdot \sigma(\Delta t)$ ($x = 1, 2, \ldots, 5$), and show that for any choice of confidence level, a 1 second window length will do the best. For events more distant than 300 km from the station, we get the same conclusion as inferred from the results of Fig. 7.6.7. It is clearly possible that a shorter time window than 1 second might further improve the P_n phase, but we have not so far investigated this possibility.

The definition of the "worst case " situation is somewhat arbitrary, but seen in conjuction with the total number of samples per day (86400), the 3σ level is a resonable practical compromise. This means that 99.9% of the data will be below this limit. We also see that for all confidence levels up to 5σ, the conclusion on the best window length for P_n will remain the same.

Similar analysis was conducted for the L_g phase. The data were bandpass filtered between 1.5 and 3.5 Hz, and the center point of the signal analysis window was set at the expected amplitude maximum of the L_g phase (i.e., at a group velocity of 3.5 km/s). To accomodate for uncertainties in the positioning of the amplitude maximum, we used a time tolerance of ± 5 seconds. Details on the L_g phases are given in Table 7.6.3, and the values of $S(\Delta t)$ for events at various distances are shown in Fig. 7.6.8. Also in this case events above and below 300 km show different slopes, and we will in the following proceed with the averages for these two populations.

The data intervals of Table 7.6.4 were also used to assess the noise characteristics of the 1.5-3.5 Hz frequency band. The estimated curves for $\overline{A}(\Delta t)$ are given in Fig. 7.6.9, and the corresponding σ-values are given in Fig. 7.6.10.

The noise damping, computed from "an average" L_g signal within 300 km epicentral distance and from "average" noise conditions, is given in Fig. 7.6.11. When considering the levels 3σ and higher, all window lengths of 5 seconds or less seem to do almost equally well. The corresponding curves for events exceeding 300 km epicentral distance are shown in Fig. 7.6.12. They indicate that an STA window length of 10 seconds will be close to optimum for all confidence levels up to 5σ.

Our preliminary assessment is that a 5 second window length should be used for L_g phases originating from events within 300 km epicentral distance, whereas a 10 second window should be used for events exceeding 300 km.

An increase in the time tolerances will increase the values of $\overline{A}(\Delta t)$, whereas $\sigma(\Delta t)$ will decrease. Fig. 7.6.13 illustrates this for a noise sample in the 1.5-3.5 Hz frequency band using a 10 second STA window length. We see that the value of $\overline{A}(\Delta t)+3\cdot\sigma(\Delta t)$ remain almost constant for any time tolerance, implying that the results we obtained with a time tolerance of $\pm$ 5 seconds, also seem to be valid for other choices of time tolerances.

Steering delays and effects of mis-steering

One of the main features of seismic arrays is the ability to improve the signal-to-noise ratio (SNR) by beamforming. Instead of computing the STA's from bandpass filtered single component sensors, we steer beams towards each target point, filter them in the appropriate frequency bands, and finally compute the

STA values. In this way, we significantly reduce the noise levels (for uncorrelated noise, by a factor of $\sqrt{N}$, where N is the number of sensors). Kværna (1989) have estimated the SNR gain, the noise suppression and the signal loss for P-phases, using data from the NORESS array. In the 3-5 Hz frequency band, appropriate for P_n, it was found that an SNR gain of 12 dB could be achieved with optimum plane-wave steering delays. It was also found that even though the array was steered with optimum steering parameters, the signal amplitudes were reduced by the beamforming, due to lack of coherency.

As shown in Fig. 7.6.14, the steering delays (apparent velocity and azimuth) appropriate for the target point, will not be optimum for the rest of the points within the surrounding rectangle. We will in the following consider the "worst case" situation, and account for the maximum signal loss for any points within the rectangle. If we assume that the expected slownesses of all points within the rectangle is identical, which is resonable for P_n and L_g, the mis-steering will primarily be caused by deviating azimuths, as shown in Fig. 7.6.14.

Fig. 7.6.15 illustrate the loss of the maximum STA as a function of mis-steering, for NORESS and ARCESS P-beams filtered between 3.0 and 5.0 Hz. Information on the events are given in Table 7.6.5. The apparent velocity of each phase is taken from broad-band f-k analysis, the STA length is one second, and the time tolerance is ± 5 seconds. The mis-steering is introduced as azimuth deviations normalized relative to an apparent velocity of 8.0 km/s. Let θ_n denote the azimuth deviation relative to an apparent velocity of 8.0 km/s and let v_p denote the apparent velocity of the incoming wave. If θ_{obs} is the azimuth deviation relative to v_p, we get the following relation:

$$\theta_{obs} = 2 \arcsin\left(\frac{v_p}{8.0} \sin \frac{\theta_n}{2}\right) \tag{6}$$

Fig. 7.6.15 shows that the signal loss is about 4 dB for a normalized azimuth mis-steering of 20 degrees. I.e., if our grid is constructed in such a way that the maximum allowed azimuth deviation is within 20 degrees (see Fig. 7.6.14), the P_n signal loss at NORESS and ARCESS will be within 4 dB. For arrays with smaller radius (e.g., FINESA), the signal loss will be less.

We have not so far investigated the signal loss due to azimuth mis-steering of the L_g phases. The apparent velocity is lower than for P_n, which indicate higher signal loss, but the lower frequency filter used for L_g (1.5-3.5 Hz versus 3.0-5.0 Hz) works in the opposite direction.

Due to the large regional variations in propagation characteristics, it is usually difficult to predict the apparent velocities, given the coordinates of the target point. Table 7.6.6 gives the estimated apparent velocity of the first arriving P-phase (P_g or P_n) as a function of epicentral distance. These statistics are taken from the IAS data base, and contain both NORESS and ARCESS observations.

Similar statistics on the L_g phase are given in Table 7.6.7. Both tables show a large scatter, illustrating the difficulty in predicting the apparent velocity given the epicentral distance. Another complicating factor is the dispersion of the L_g wave train, implying that the estimates of apparent velocity will be a function of both the frequency band and the positioning of the analysis window.

We have initially not attempted to do any systematic regionalization of the apparent velocity observations. In the mean time, we use an apparent velocity of 8.0 km/s when forming P_n beams steered towards target points more distant that 250 km. At closer distances, we use 6.5 km/s. For L_g beams, an apparent velocity of 4.3 km/s is assumed for target points at all distances. These parameters are currently used for all arrays (NORESS, ARCESS and FINESA).

The signal loss will also be dependent on the array geometry, but this has so far not been studied in connection with mis-steering of the beams. A natural next step will be to evaluate all the effects of beamforming, array geometries and mis-steering in the context of threshold monitoring. But in this preliminary study, the signal loss is accounted for by adding a constant term of 0.2 (4 dB) to the observed $\log(STA)$ values for P_n (P_g), and 0.3 (6 dB) to the $\log(STA)$ values for L_g

Magnitude correction factors and variance

We are now in the position to compute the generic relations for the magnitude correction factors, as the other TM variables have been preliminary assessed. Alsaker *et al* (1990), collected a large event data base when estimating formulas for a M_L scale in Norway, and they subsequently computed network averaged M_L estimates for all events. We will in the following use their data base and magnitudes as a basis for computing the generic relations for the magnitude correction factors.

The data base contains observations from 21 different stations (see Fig. 7.6.16), most of which with different instrument response functions. In order to compare the STA values at the respective stations, we need to find a common basis for comparison. As the individual amplitude response functions show only small variations within the relatively narrow passbands considered for P_n and L_g, we can in an approximate way transfer the STA values into units of nm or nm/s simply by multiplying by the displacement or velocity response at the center frequency of the passband, such that

$$STA_{nm} \approx STA_{qu} \cdot |A_d(\omega_c)| \tag{7}$$

where STA_{qu} is the observed STA in quantum units, $|A_d|$ is the displacement amplitude response, and the center frequency $\omega_c = \sqrt{\omega_1 \omega_2}$ where ω_1 and ω_2 are the low and high cutoffs of the passband. A similar type of equation can be used

if we instead convert the STA values to ground velocity.

In accordance with earlier regression analysis of magnitude relations (Alsaker *et al*, 1990), we choose the following parameterizition:

$$M_i = \log STA_i + C1 + C2 \cdot \log \Delta_i + C3 \cdot \Delta_i \qquad (i = 1, \cdots, N) \qquad (8)$$

where N is the number of observations, M_i is the network magnitude of the event, STA_i is the instrument corrected STA_{nm} and Δ_i is the epicentral distance.

The data base of Alsaker *et al* (1990) contains 741 observations distributed among 195 events (see Fig. 7.6.17). To ensure good SNR in the P_n and L_g frequency bands, all data were visually inspected. After rejecting data with insufficient SNR or with other data quality problems, 453 observations remained for P_n analysis and 528 for L_g. The STA values were computed using the recipes outlined in the preceding sections, and the results from the regression analyses are given in Table 7.6.8. Estimates of the standard deviation are also given, and show a σ value of 0.19 for L_g. The P_n data show a much larger scatter, and we obtained a σ value of 0.36. Compared to site specific monitoring, these σ estimates are significantly higher, as the typical σ values for site specific monitoring are less than 0.2 for P_n, and less than 0.1 for L_g. If different filters, travel-time models or other parameters were to be used in the TM analysis, new magnitude correction factors would have to be obtained from reanalysis of the calibration events, using the new recipies.

As the TM method computes upper magnitude limits from a cumulative distribution with a given mean and standard deviation, we have the option of balancing the term $C1$ against the standard deviation σ. This implies that we can reduce σ if $C1$ is increased. Our philosophy behind the TM computations has been to make conservative estimates of the upper magnitude limits, in order not to overestimate the capabilities. In this way, we can add a constant term to $C1$ or increase σ if some of the attenuation relations or other underlying parameter estimates of the TM method are considered particularly uncertain.

Discussion

The results presented in this study give us a means of testing the concept of threshold monitoring applied to large geographical regions. It enables us to extend the original "site-specific" threshold monitoring to what we might call "regional threshold monitoring". Using these initial generic relations, Ringdal and Kværna (1991, this issue) have already shown how colour computer displays can be applied to interpret the results from TM analysis. They also indicate new applications of the regional threshold monitoring concept which should be investigated in parallel with improvements of the generic relations.

The data base used for obtaining the magnitude calibration factors consists of

events from Fennoscandia and adjacent areas, making the results representative for this kind of geological environment. If we want to extend the TM analysis to other types of geological regions, exhibiting different wave propagations characteristics, new generic relations have to be found. Another uncertain factor, concerning the current magnitude calibration factors, is the effect of using this particular data base for regression, as the same data base was used for obtaining the M_L scale for Norway (Alsaker *et al*, 1990).

The effect of signal loss due to mis-steering of the arrays should be more thoroughly investigated. The signal loss is a function of several variables, among others; phase type, signal coherency, frequency, degree of mis-steering and array geometry. This also implies that when new arrays, with different array geometries, are introduced in the TM computations, new models for signal loss have to be assessed.

We are also investigating the possibility of using several filter bands when representing the amplitude level of a phase. The current model of a fixed frequency band for P_n and L_g is clearly not optimal. But in order to make such improvements, new generic relations have to be obtained for a set of different filter bands.

Regionalization of the travel-time models for the maximum amplitude peaks in the wavetrain will optimize the TM computations. The data base of Alsaker *et al* (1990) contains several recordings at NORESS and ARCESS which can be used to regionalize the travel-time models at these two stations. But for the other stations currently providing digital data to NORSAR (FINESA, GERESS, Ksiaz and Stary Folwark), a new event data base will have to be collected. If independent network averaged magnitudes can be provided for these events, the generic relations for magnitude calibration can also be improved.

In conclusion, the key for further improvements of the generic relations for regional theshold monitoring is easy access to a large event data base including recordings at all relevant stations. Network locations and network averaged magnitudes should be avaliable for all events. With this at hand, we have the possibility to investigate regional behaviour and the effect of different parameter settings, in order to further improve the performance of regional threshold monitoring.

Tormod Kværna

References

Alsaker, A., L.B. Kvamme, R.A. Hansen, A. Dahle and H. Bungum (1991): The M_L scale in Norway, *Bull. Seism. Soc. Am.* Vol. 81, No. 2, In press.

Bache, T., S.R. Bratt, J. Wang, R.M. Fung, C. Kobryn and J.W. Given (1990), The Intelligent Monitoring System, *Bull. Seism. Soc. Am.* 80, Part B, 1833-1851.

Baumgardt, D.R., (1990), Investigation of Teleseismic L_g Blockage and Scattering Using Regional Arrays, *Bull. Seism. Soc. Am.* 80, Part B, 2261-2281.

Båth, M. (1981): Local magnitude — recent research and current trends, *Earth-Science Rev.* 17, 315-398.

Kværna, T. and S. Mykkeltveit (1985): Propagation characteristics of regional phases recorded at NORSAR, *Semiannual Tech. Summary, 1 Apr - 30 Sep 1985,* NORSAR Sci. Rep. 1-85/86, NORSAR, Kjeller, Norway.

Kværna, T. and F. Ringdal (1990a): Application of the threshold monitoring method, *Semiannual Tech. Summary, 1 Oct 1989 - 31 Mar 1990,* NORSAR Sci. Rep. 2-89/90, NORSAR, Kjeller, Norway.

Kværna, T. and F. Ringdal (1990b): Continuous threshold monitoring of the Novaya Zemlya test site, *Semiannual Tech. Summary, 1 Apr - 30 Sep 1990,* NORSAR Sci. Rep. 1-90/91, NORSAR, Kjeller, Norway.

Richter, C.F. (1935): An instrumental earthquake magnitude scale, *Bull. Seism. Soc. Am.* 25, 1-32.

Ringdal, F. and T. Kværna (1989): A multi-channel processing approach to real-time network detection, phase association, and threshold monitoring, *Bull. Seism. Soc. Am.* 79, 1927-1940.

Ringdal, F. and T. Kværna (1991): Continuous threshold monitoring using "regional thresholds displays", This volume.

Sereno, T.J., (1991): Simulation of the detection and location capability of regional seismic networks in the Soviet Union, *Final Report, 1 Jan 1989 - 31 Dec 1990, SAIC-91/1061* Sci. Appl. Int. Corp., San Diego, Calif., USA.

	0-250	250-500	500-750	750-1000	1000-1250	1250-1500	1500-1750	1750-2000	Total
1.0-2.0Hz	2	5	0	18	4	5	1	1	36
2.0-3.0Hz	153	264	24	88	94	59	10	4	696
3.0-4.0Hz	245	922	77	224	97	131	21	7	1724
4.0-5.0Hz	562	1991	160	243	245	100	13	3	3317
5.0-6.0Hz	351	670	61	85	93	13	1	1	1275
6.0-7.0Hz	513	523	74	98	62	5	1	1	1277
7.0-8.0Hz	183	121	27	21	7	0	0	0	359
8.0-9.0Hz	367	180	45	29	16	2	0	0	639
9.0-10.0Hz	284	179	56	31	9	1	1	0	561
Total	2660	4855	524	837	627	316	48	17	9884

Table 7.7.1. This table gives an overview of the frequencies with the highest SNR for the first arriving P-phase (P_n or P_g). Each element of this table, give the number of observations of the dominant frequency for a given frequency and distance range. The data are taken from routine detection processing of the IAS system, and the statistics cover both NORESS and ARCESS data from the time interval 1990/01/23 to 1991/04/29. All events were below M_L 3.0. The frequency band 3-5 Hz found suitable for TM analysis of P_n or P_g data is outlined by two horizontal lines.

	0-250	250-500	500-750	750-1000	1000-1250	1250-1500	1500-1750	1750-2000	Total
0.5-1.5Hz	34	22	9	91	26	34	0	0	216
1.5-2.5Hz	105	516	122	340	145	24	2	0	1254
2.5-3.5Hz	327	1595	162	166	34	8	1	0	2293
3.5-4.5Hz	671	1426	32	13	11	3	0	0	2156
4.5-5.5Hz	733	738	11	4	6	2	0	0	1494
5.5-6.5Hz	154	116	0	0	2	0	0	0	272
6.5-7.5Hz	324	150	4	0	3	0	0	0	481
7.5-8.5Hz	106	25	0	1	0	0	0	0	132
8.5-9.5Hz	148	21	3	0	0	0	0	0	172
9.5-10.5Hz	50	20	1	0	0	0	0	0	71
Total	2652	4629	344	615	227	71	3	0	8541

Table 7.7.2. Same as Table 7.7.1, but for the L_g phase. The frequency band 1.5-3.5Hz found suitable for TM analysis of L_g data is outlined by two horizontal lines.

Origin time	Lat.	Long.	Distance	M_L	Station	P_n data	L_g data
1990-101:11.51.55.4	62.8	27.6	170.8	-	FINESA	yes	yes
1990-101:13.46.07.0	60.9	29.3	183.8	-	FINESA	yes	yes
1989-167:11.23.26.0	69.4	30.6	200.0	3.0	ARCESS	yes	yes
1989-076:11.48.53.0	69.4	30.6	200.0	2.9	ARCESS	yes	yes
1990-101:10.21.21.0	59.5	25.0	224.8	-	FINESA	yes	yes
1989-033:18.28.55.0	67.1	20.6	338.5	2.5	ARCESS	yes	yes
1989-059:18.36.45.0	67.1	20.6	338.5	2.5	ARCESS	yes	yes
1989-105:08.50.53.0	68.1	33.2	348.9	2.7	ARCESS	yes	yes
1989-133:08:18.49.0	68.1	33.2	348.9	2.7	ARCESS	yes	yes
1988-258:08.59.58.0	64.7	30.7	584.0	2.9	ARCESS	yes	yes
1988-141:09.54.24.0	59.5	25.0	760.0	2.7	NORESS	no	yes
1989-051:13.19.57.0	59.5	25.0	760.0	2.5	NORESS	no	yes
1989-108:13.41.15.0	59.5	26.5	841.0	2.8	NORESS	no	yes
1988-075:11.52.22.0	61.9	30.6	882.2	2.8	ARCESS	yes	yes
1990-103:10.18.55.0	59.2	28.1	937.0	3.1	NORESS	yes	no
1989-005:10.09.07.0	61.9	30.6	1024.3	2.5	NORESS	no	yes
1988-258:08.59.58.0	64.7	30.7	1069.4	2.9	NORESS	no	yes
1990-103:10.28.41.0	64.6	31.2	1093.7	3.0	NORESS	yes	no
1989-090:12.16.17.0	59.5	26.5	1119.8	3.0	ARCESS	no	yes
1990-103:08.37.08.0	67.6	33.5	1302.7	2.8	NORESS	yes	no
1989-167:11.23.26.0	69.4	30.6	1307.3	3.0	NORESS	no	yes
1989-168:08.59.23.0	68.1	33.2	1314.3	2.9	NORESS	no	yes

Table 7.7.3. Information on the events used for computation of maximum signal amplitudes, denoted $S(\Delta t)$.

Start time	Station
1990-096:22.50.00	NORESS
1990-096:23.00.00	ARCESS
1990-097:14.30.00	NORESS
1990-097:14.30.00	ARCESS
1990-099:09.00.00	NORESS
1990-099:09.00.00	ARCESS

Table 7.7.4. Start times of noise intervals used for assessing average noise characteristics. The length of all intervals were 30 minutes

Origin time	Lat.	Long.	Station	Arrival time	Azimuth	App. vel.	SNR
1991-119:11.25.26.0	56.2	11.5	NORESS	1991-119:11.26.35.9	185.2	8.8	58.8
1991-120:03.40.34.0	51.4	16.2	NORESS	1991-120:03.42.53.4	156.9	8.6	33.0
1991-120:09.19.37.0	67.9	34.3	ARCESS	1991-120:09.20.35.1	120.4	7.8	128.4
1991-120:11.59.23.0	64.6	32.0	ARCESS	1991-120:12.00.45.3	154.3	8.7	54.1
1991-120:12.34.46.0	69.4	31.0	ARCESS	1991-120:12.35.19.7	94.4	7.7	283.4

Table 7.7.5. List events used for the preliminary assessment of signal loss due to mis-steering of the P-beams. The event locations are the automatic network solutions from the generalized beamforming method, see Ringdal and Kværna (1989).

	0-250	250-500	500-750	750-1000	1000-1250	1250-1500	1500-1750	1750-2000	Total
6.0-6.5km/s	194	56	2	2	1	2	0	0	257
6.5-7.0km/s	808	485	8	3	2	2	0	0	1308
7.0-7.5km/s	599	1487	28	27	7	13	0	0	2161
7.5-8.0km/s	482	1479	61	77	62	33	11	1	2206
8.0-8.5km/s	372	664	107	86	171	69	14	4	1487
8.5-9.0km/s	140	380	111	122	158	79	10	1	1001
9.0-9.5km/s	32	181	71	107	78	61	4	1	535
9.5-10.0km/s	13	76	54	99	56	27	4	4	333
10.0-10.0km/s	6	17	24	108	24	12	1	2	194
10.5-11.0km/s	6	10	16	95	32	7	2	0	168
11.0-11.0km/s	3	6	18	47	13	2	1	0	90
11.5-12.0km/s	2	6	7	23	8	1	0	2	49
Total	2657	4847	507	796	612	308	47	15	9789

Table 7.7.6. This table give an overview of the estimated apparent velocity of the first arriving P-phase (P_n or P_g). Each element of this table, give the number of observations of the apparent velocity for a given apparent velocity and distance range. The data are taken from routine detection processing of the IAS system, and the statistics cover both NORESS and ARCESS data from the time interval 1990/01/23 to 1991/04/29. All events were below M_L 3.0.

	0-250	250-500	500-750	750-1000	1000-1250	1250-1500	1500-1750	1750-2000	Total
2.5-2.8km/s	0	6	0	0	1	1	0	0	8
2.8-3.1km/s	52	108	18	21	31	5	1	0	236
3.1-3.4km/s	41	446	34	39	59	5	0	0	624
3.4-3.7km/s	154	358	45	66	35	4	0	0	662
3.7-4.0km/s	616	832	83	168	40	20	1	0	1760
4.0-4.3km/s	913	1335	80	211	25	20	0	0	2584
4.3-4.7km/s	480	883	45	85	20	9	1	0	1523
4.7-5.0km/s	208	434	16	20	8	4	0	0	690
5.0-5.3km/s	112	165	10	4	4	2	0	0	297
5.3-5.5km/s	58	36	5	0	2	0	0	0	101
Total	2634	4603	336	614	225	70	3	0	8485

Table 7.7.7. Same as Table 7.7.6, but for the L_g phase.

Phase	$C1$	$C2$	$C3$	σ	nobs
P_n, P_g	-1.5737	1.4236	0.6819E-03	0.355	453
L_g	-0.9537	0.8292	1.3188E-03	0.192	528

Table 7.7.8. Results from regression analysis of the data used by Alsaker *et al* (1990). The regression coefficients and the σ values for P_n (P_g) and L_g were obtained from processing the data with the TM recipies outlined in the preceding sections.

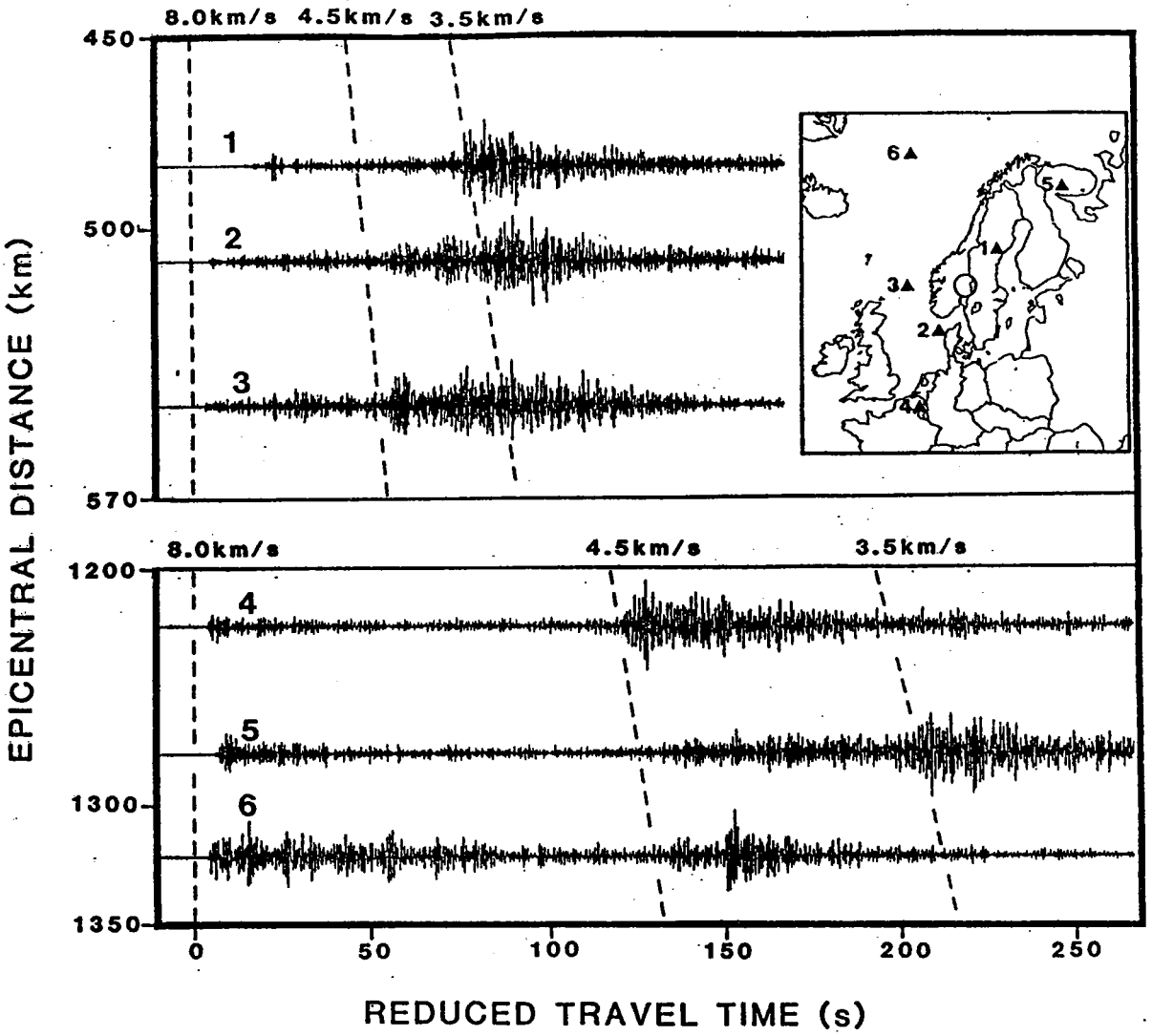

Fig. 7.7.1. Illustration of variation of relative importance of the phases S_n and L_g. The standard group velocities of 4.5 and 3.5 km/s, commonly assigned to S_n and L_g, respectively, are marked by dashed lines. The upper three traces cover the distance interval 480-550 km, while the three lower traces correspond to epicentral distances in the range 1225-1320 km. The location of the NORSAR array is denoted by a ring on the map, and the traces are from the NORSAR seismometer 02B01. The data are bandpass filtered 1 to 5 Hz. The reduction velocity is 8.0 km/sec.

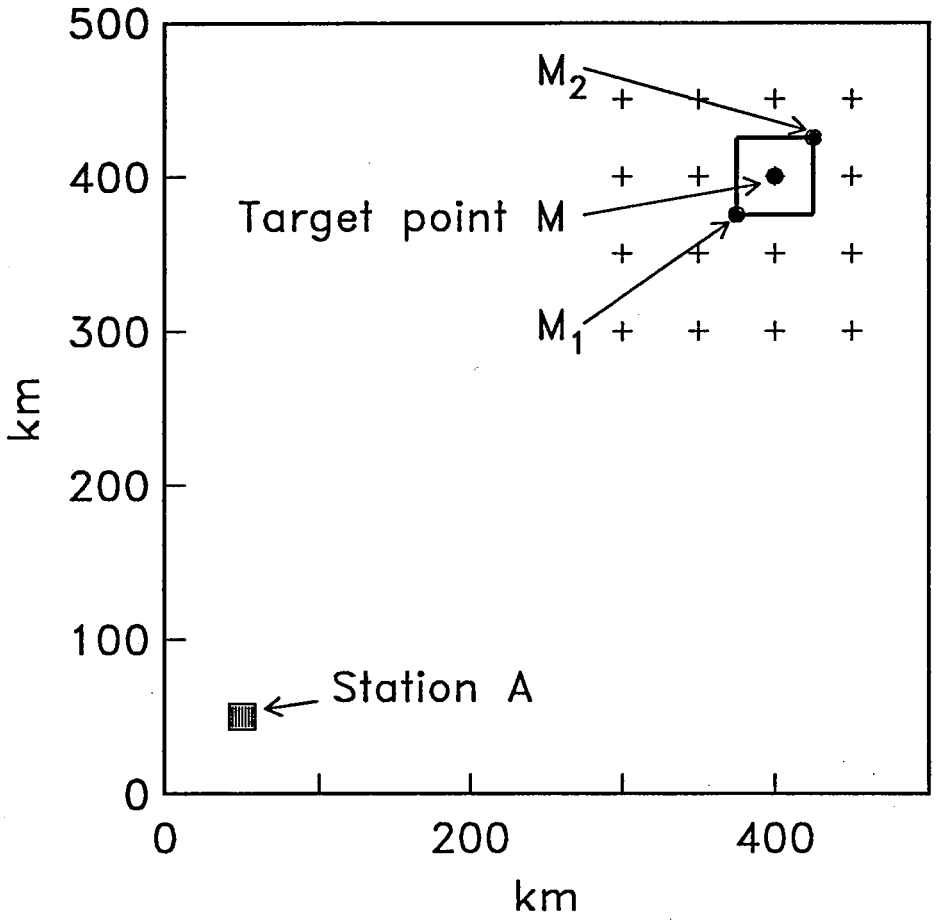

Fig. 7.7.2. This figure illustrates the necessity of using time tolerances. The plus signs indicate target points, and a rectangle surrounding one of the target points (M) is also given. The point within the rectangle with the minimum travel-time is denoted M_1, whereas the point with the maximum travel-time is denoted M_2.

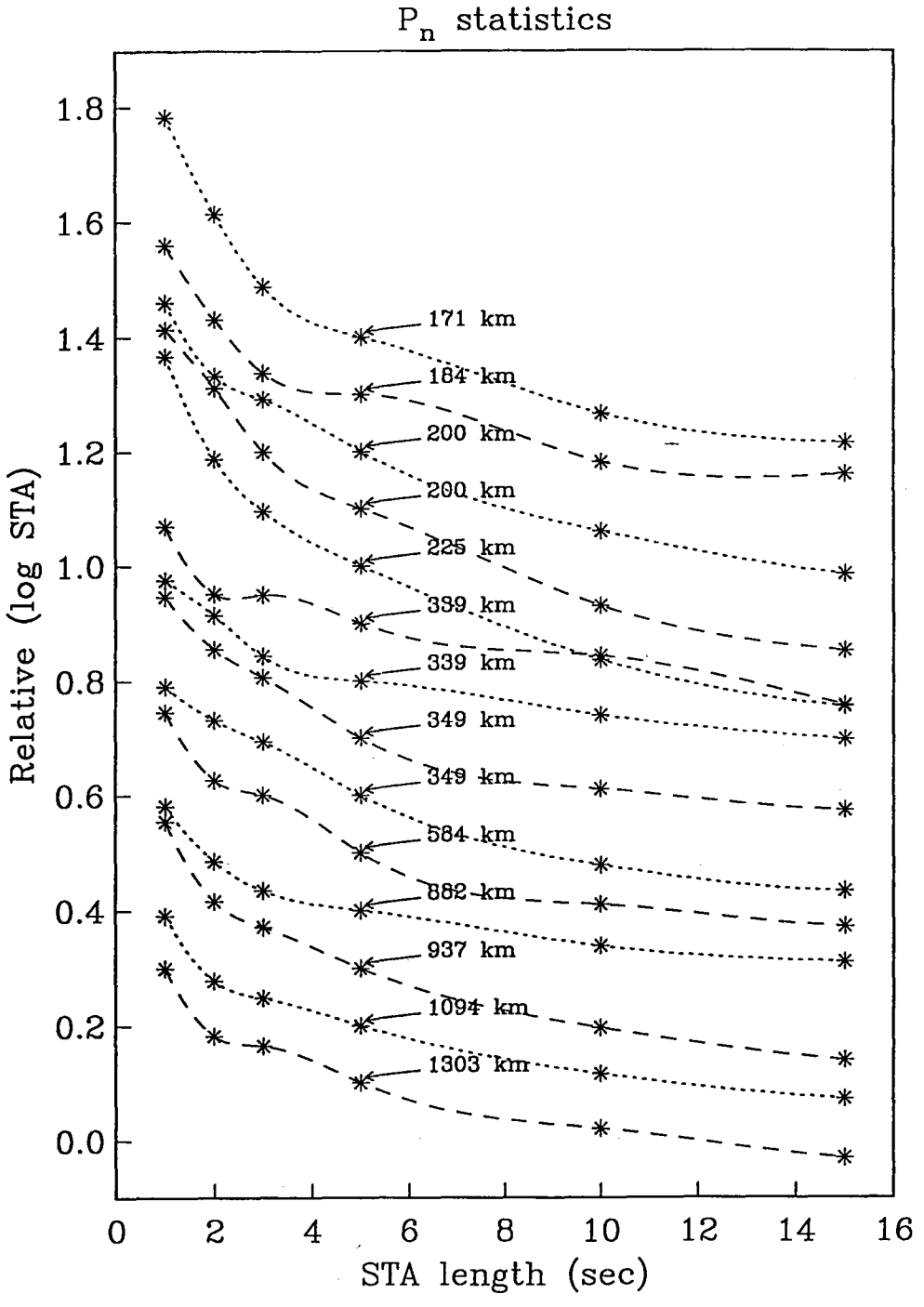

Fig. 7.7.3. The asterisks of this figure show observations of maximum $\log(STA)$ (denoted $S(\Delta t)$) for P_n for a set of STA lengths. The observations corresponding to the same phase are interpolated by dashed or dotted lines, and the epicentral distance of each event is indicated. Information on the events are given in Table 7.7.3. For display purposes an offset was added to each of the curves, as the absolute scale is without any significance. Note the difference in the slopes for events above and below 300 km epicentral distance.

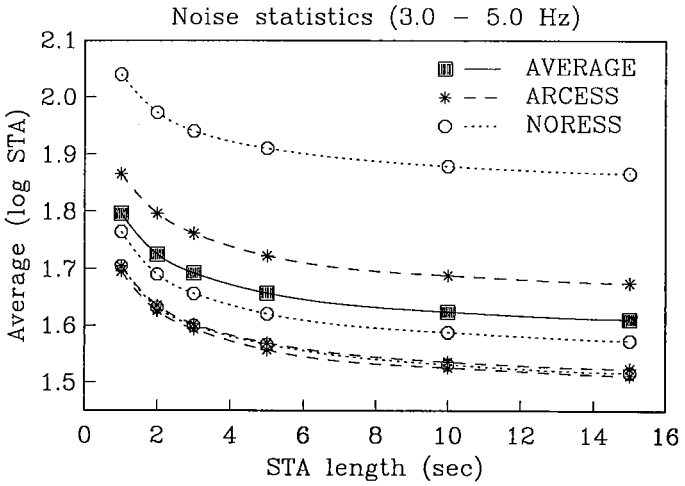

Fig. 7.7.4. Using data from the center instrument A0 of both the NORESS and the ARCESS array, this figure shows the average of $\log(STA)$ under noise conditions (denoted $\overline{A}(\Delta t)$) for a set of STA lengths. The data were filtered in the passband 3-5 Hz and a time tolerance of ± 5 seconds was used. Information on the data intervals is given in Table 7.7.4. The average of the six noise observations, used for subsequent analysis of noise damping, is indicated by filled squares and a solid line.

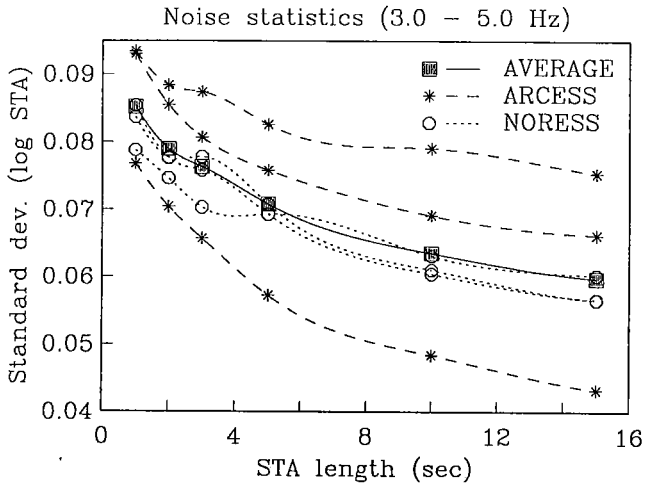

Fig. 7.7.5. This figure gives the standard deviation of the noise observations analyzed in Fig. 7.7.4. The average of the standard deviation curves, used for subsequent analysis of noise damping, is indicated by filled squares and a solid line.

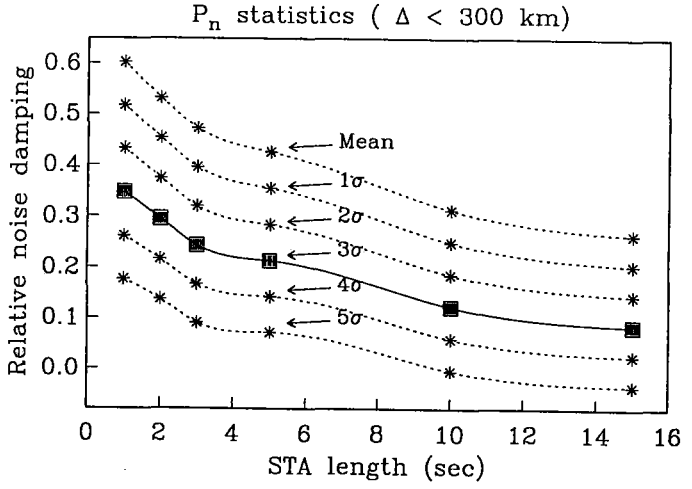

Fig. 7.7.6. The relative noise damping given in this figure is computed from average P_n signal behavior for events within 300 km epicentral distance (taken from Fig. 7.7.3), average noise conditions (taken from Fig. 7.7.4) and average values of noise standard deviation (taken from Fig. 7.7.5). The relative noise damping for a set of confidence levels is shown and the 3σ level used to characterize a "worst case" situation is given by filled squares and a solid line.

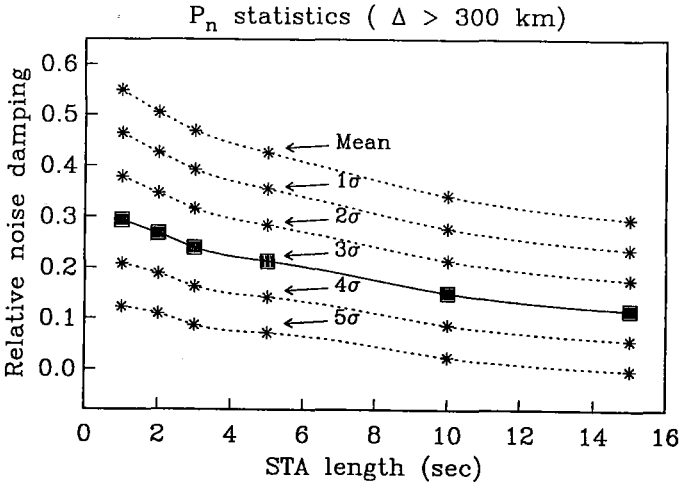

Fig. 7.7.7. Same a Fig. 7.7.6, but representing events with epicentral distances exceeding 300 km.

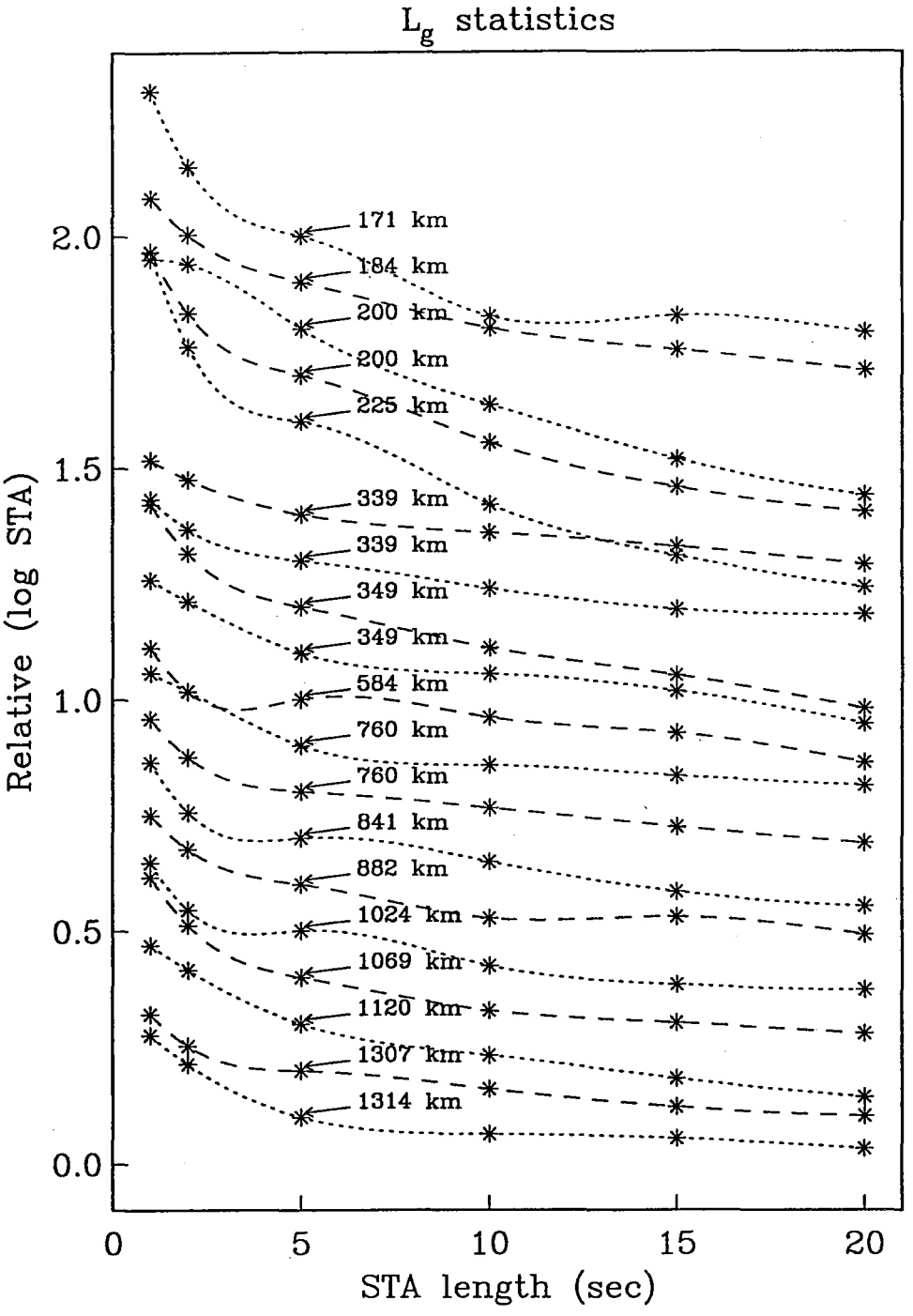

Fig. 7.7.8.. The asterisks of this figure show observations of maximum $\log(STA)$ (denoted $S(\Delta t)$) for L_g for a set of STA lengths. The observations corresponding to the same phase are interpolated by dashed or dotted lines, and the epicentral distance of each event are indicated. Information on the events is given in Table 7.7.3. For display purposes an offset was added to each of the curves, as the absolute scale is without any significance. Note the difference in the slopes for events above and below 300 km epicentral distance.

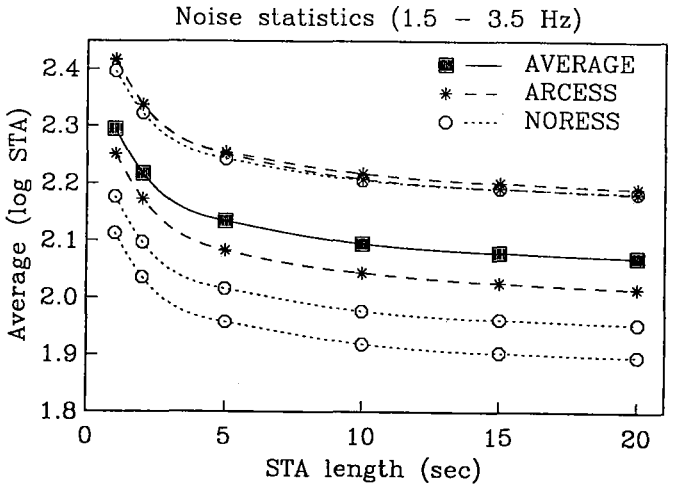

Fig. 7.7.9. Same a Fig. 7.7.4, but the noise intervals were analyzed in the 1.5-3.5 Hz filter band.

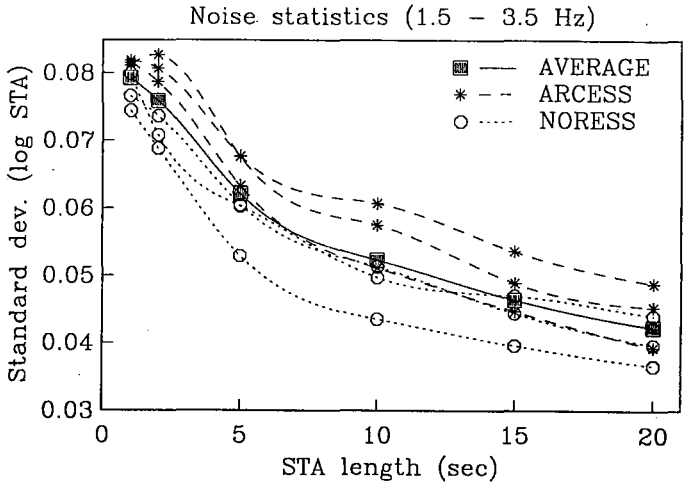

Fig. 7.7.10. This figure gives the standard deviation of the noise observations analyzed in Fig. 7.7.9. The average of the standard deviation curves, used for subsequent analysis of noise damping is indicated by filled squares and a solid line.

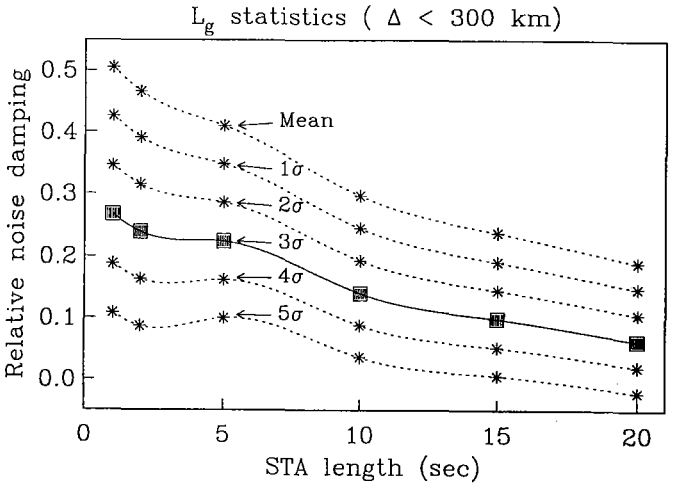

Fig. 7.7.11. The relative noise damping given in this figure is computed from average L_g signal behaviour for events within 300 km epicentral distance (taken from Fig. 7.7.8), average noise conditions (taken from Fig. 7.7.9) and average values of noise standard deviation (taken from Fig. 7.7.10). The relative noise damping for a set of confidence levels is shown and the 3σ level used to characterize a "worst case" situation is given by filled squares and a solid line.

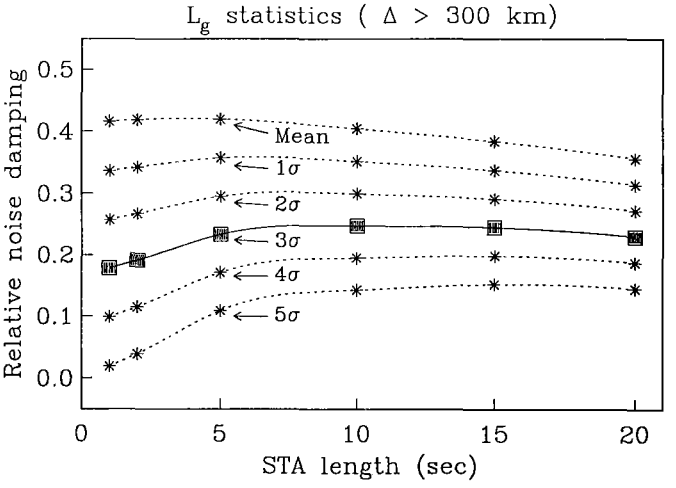

Fig. 7.7.12. Same a Fig. 7.7.11, but representing events with epicentral distances exceeding 300 km.

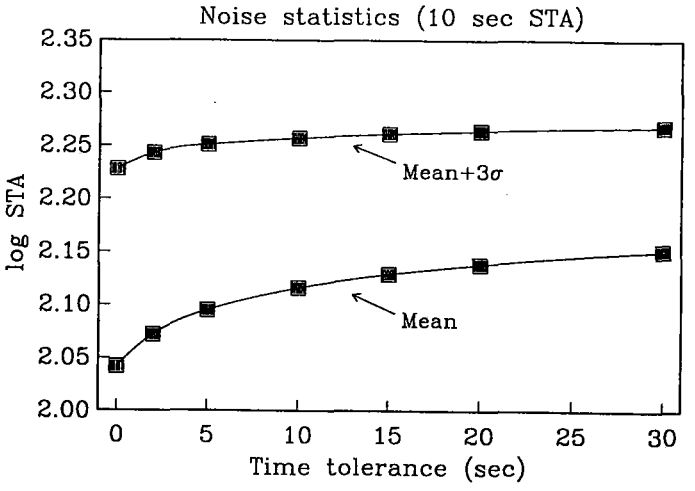

Fig. 7.7.13. This figure gives the mean of $\log(STA)$ together with the mean+3σ level for a set of time tolerances. The first noise segment of Table 7.7.4 was bandpass filtered between 1.5 and 3.5 Hz, and the estimates were obtained using an STA length of 10 seconds.

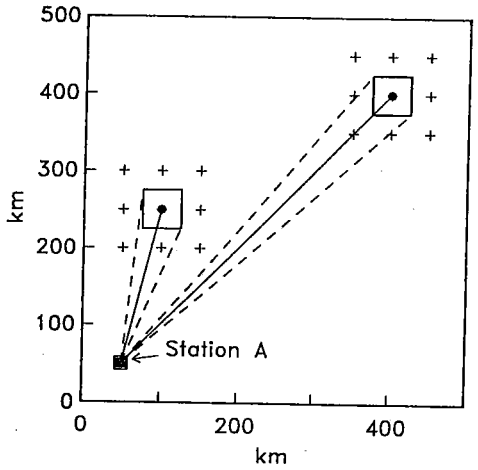

Fig. 7.7.14. In order to monitor a finite area surrounding each of the target points, a mis-steering in azimuth is introduced when the beams are steered towards the target points. This figure illustrates this for two target points at different distances. The azimuth deviations are indicated by dashed lines. Also note that for a fixed grid spacing, the mis-steering is a function of distance to the target points.

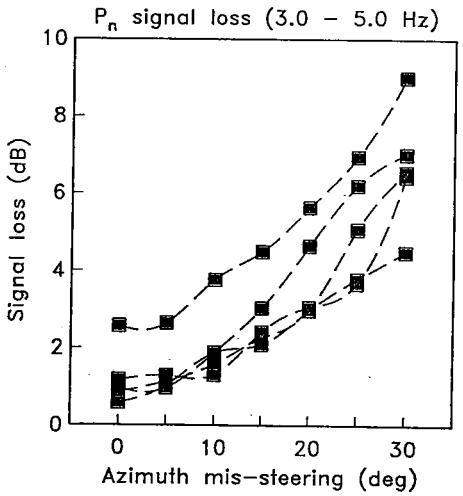

Fig. 7.7.15. The filled squares of this figure give the estimated signal loss for P_n as a function of azimuth mis-steering. Observations corresponding to the same phase are interpolated by dashed lines and information on the P-phases are given in Table 7.7.5. For a circular array, it is common to map the signal loss as a function of deviations in horizontal slowness. We have therefore computed signal losses as a function of azimuth, where the azimuth deviations are normalized to provide equal deviations in horizontal slowness. The x-axis of this plot is given as normalized azimuth deviations relative to an apparent velocity of 8.0 km/s.

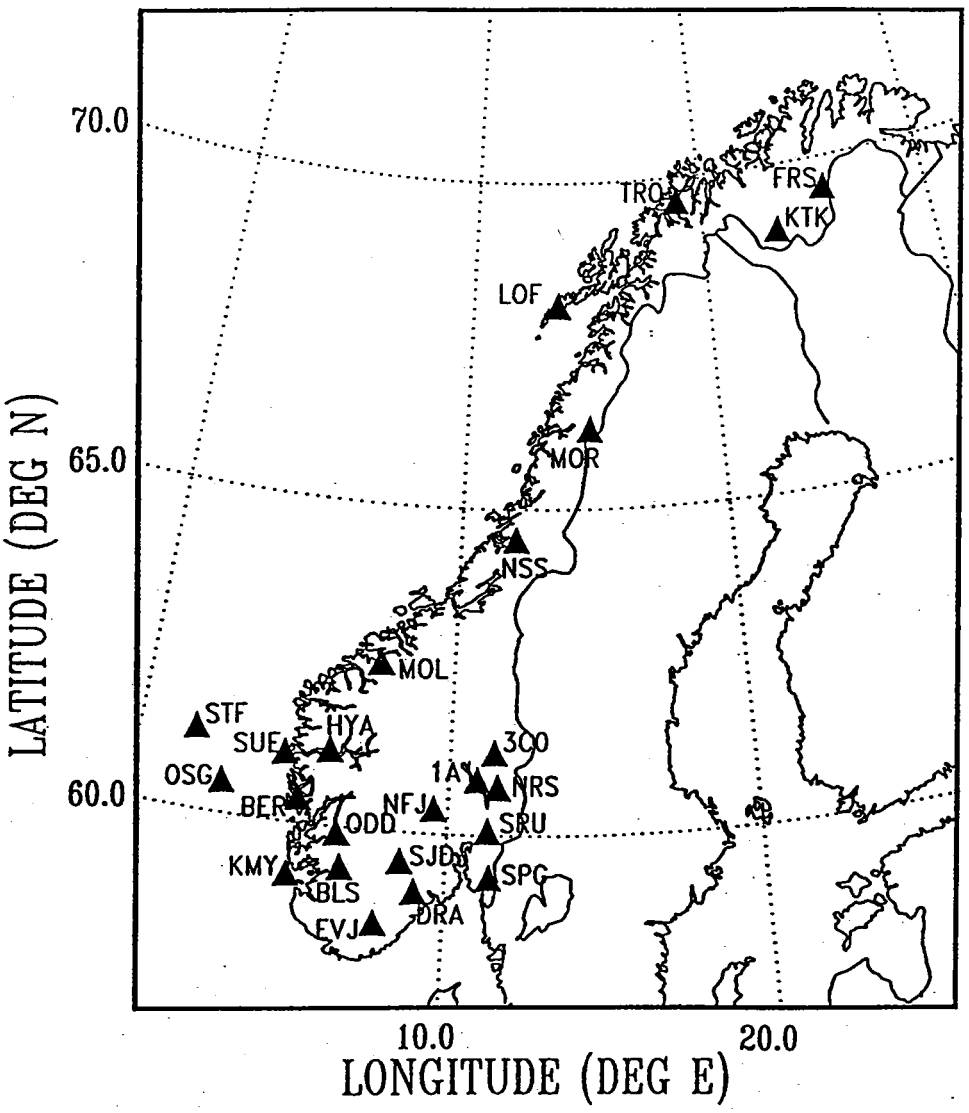

Fig. 7.7.16. Recording stations providing data for regression analysis. Adapted from Alsaker *et al* (1990).

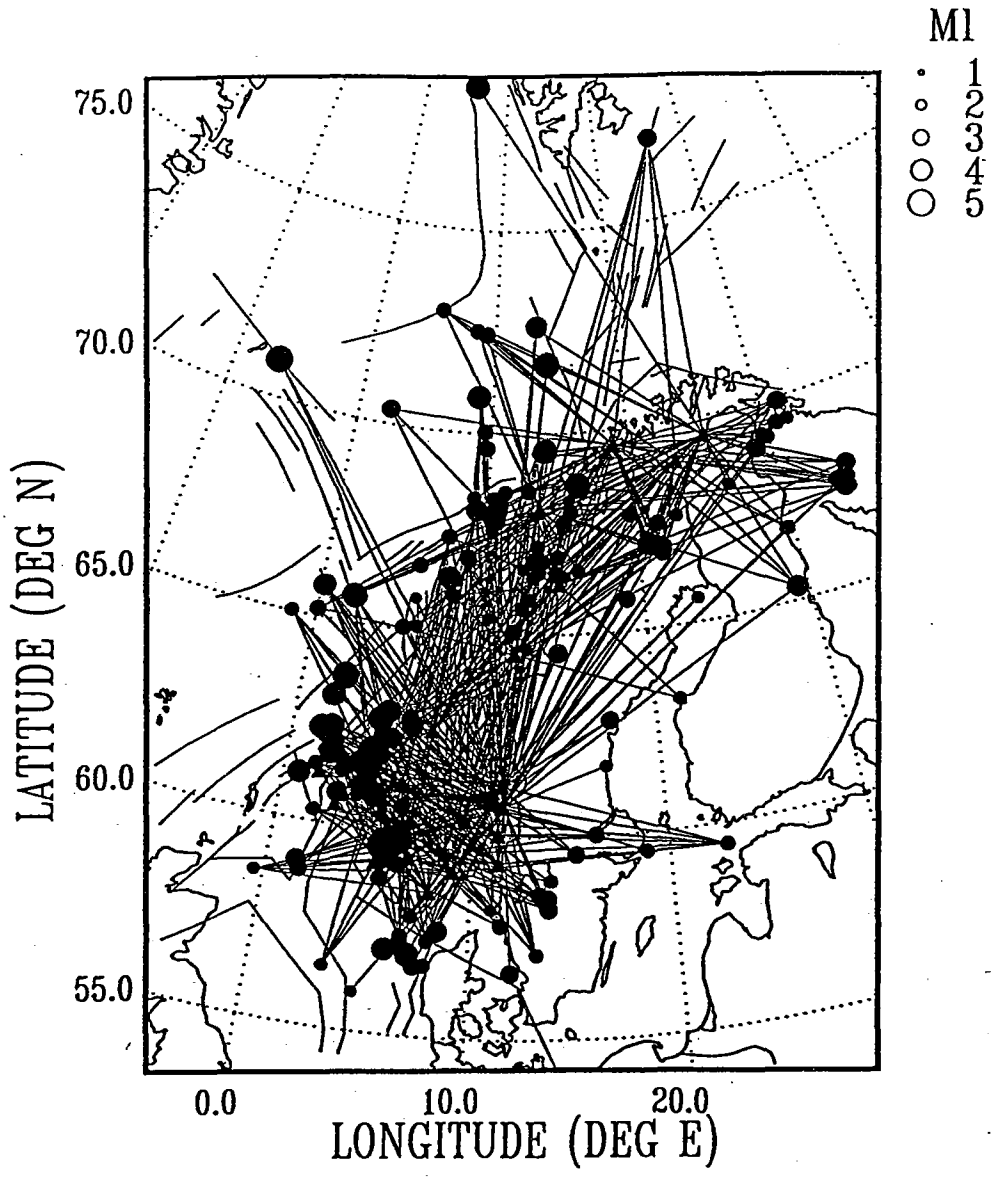

Fig. 7.7.17. Recordings selected by Alsaker *et al* (1990) for estimation of an M_L scale for Norway. Applying regression analysis, a subset of these recordings was used for obtaining generic relations for the magnitude correction factors. Adapted from Alsaker *et al*, 1990.